Int. J. Nano Dimens., 10 (2): 180-194, Spring 2019

ORIGINAL ARTICLE

Graphene Oxide/Hydroxyapatite/Silver (rGO/HAP/Ag) nanocomposite: Synthesis, characterization, catalytic and antibacterial activity

Maryam Beiranvand [1], Saeed Farhadi[1,], Abdelnassar Mohammadi[2]*

[1] *Department of Chemistry, Lorestan University, Khorramabad, Iran.*

[2] *Department of Biology, Lorestan University, Khorramabad, Iran.*

Received 12 June 2018; revised 01 November 2018; accepted 03 November 2018; available online 08 November 2018

Abstract

In this paper, a novel ternary nanocomposite namely reduced graphene oxide/hydroxyapatite/silver (rGO/HAP/Ag) was prepared by a simple hydrothermal method using graphene oxide nanosheets, $Ca(NO_3)_2$, $(NH_4)_2HPO_4$, and $AgNO_3$ as starting materials. The as-prepared nanocomposite was characterized by using various photophysical techniques including Fourier transform infrared spectroscopy (FT-IR), Raman spectroscopy, X-ray diffraction (XRD), ultraviolet-visible (UV-Vis) spectroscopy, transmission electron microscopy (TEM), scanning electron microscopy (SEM), and energy dispersive X-ray analysis (EDX). Additionally, the antibacterial and catalytic activities of the nanocomposite were evaluated. The results showed that the rGO/HAP/Ag nanocomposite exhibited high performance in the reduction of toxic nitro compounds (4-nitrophenol, 2-nitrophenol, 4-nitroaniline, and 2-nitroaniline) into the less toxic corresponding amines using $NaBH_4$ within 21-42 min with a rate constant equal to 0.1646, 0.0898, 0.1071 and 0.2 min^{-1}, respectively. Moreover, the rGO/HAP/Ag nanocomposite could be separated from the reaction mixture due to its heterogeneous nature and reused without any change in structure. In addition, the antibacterial activity of the rGO/HAP/Ag nanocomposite by disk diffusion method was evaluated against Gram-positive bacteria (*Bacillus cereus* and *Staphylococcus aureus*) and Gram-negative bacteria (*Escherichia coli* and *Klebsiella pneumonia*). The results showed that this novel ternary nanocomposite has good antibacterial activity against Gram-positive bacteria.

Keywords: *Antibacterial Activity; Graphene Oxide Nanosheets; Hydroxyapatite; Nitro Reduction; Silver Nanoparticles; Ternary Nanocomposite.*

How to cite this article

Beiranvand M, Farhadi S, Mohammadi AN. Graphene Oxide/Hydroxyapatite/Silver (rGO/HAP/Ag) nanocomposite: Synthesis, characterization, catalytic and antibacterial activity. Int. J. Nano Dimens., 2019; 10 (2): 180-194.

INTERODUCTION

Graphene oxide (GO), a single layer structure of the two-dimensional carbon material, has attracted the attention of various researchers because it has fascinating properties as electrical, thermal, and optical conductivity, high specific surface area, excellent mechanical properties, excellent charge transport mobility, high density, high electrocatalytic activity, desirable biocompatibility and low cost [1]. The presence of the oxygen-containing functional groups such as hydroxyl, epoxide, carboxyl, carbonyl functional groups on the surface of GO makes it to be highly hydrophilic. Furthermore, these functional groups can be used as the chemical anchoring sites for the nanoparticles attachment to generate new composite materials with enhanced properties [2].

Hydroxyapatite [$Ca_{10}(PO_4)_6(OH)_2$, HAP], having the main mineral constituent of vertebrate bones and teeth, is a well-known calcium phosphate bioceramics [3-5]. Hydroxyapatite is utilized in a wide variety of applications such as biomedical devices as bone substitute materials because of its favourable biological properties. Some of these properties include excellent biocompatibility, bioactivity, osteoconductivity, bioaffinity, slow

* Corresponding Author Email: *sfarhadi1348@yahoo.com*

biodegradability, non-toxic, osteointegration and osteoinduction in certain conditions, with a crystallographic and chemical composition similar to that of the inorganic constituent of natural bone [6]. Besides, HAP is used in middle ear implants [7], tissue engineering systems [8], drug delivery agent [9], dental materials [10] and bioactive coating on metallic osseous implants [11]. Moreover, outside the biomedical field, HAP is applied as a catalyst for the chemical reactions [12], ion conductors [13], gas sensors [14] proteins and nucleic acids chromatography [15], water treatment processes [16] and the remediation of heavy metal contaminated soils [17]. However, the pure HAP is suitable only for the repair of non-load-bearing bones because of its fragility, low mechanical strength, easy rupture and weak fatigue resistance; it cannot withstand the normal operating loads of bone or joints. To improve its mechanical property for practical application, the composites of HAP and other compounds including ceramics, polymers, metals and inorganics have been developed [18]. Some researchers have shown that by combining HAP particles with natural or synthetic nanofibers, the mechanical strength of HAP may be increased. For instance, polyamide 6/HAP nanocomposite was synthesized via in situ hydrolytic ring-opening polymerization of ε-caprolactam in the presence of newly synthesized HAP aqueous slurry [19]. HAP/poly (ethylene co vinyl alcohol) (EVA) nanocomposite was synthesized by a solution-based chemical methodology with varying HAP contents from 10 to 60 % (w/w) [20]. In addition, a synthesis of poly (vinyl alcohol-co-lactic acid, PVA-co-LA)/HAP composite was reported [21]. Chitosan/HAP nanocomposites have been prepared by solvent casting their hybrid suspensions [22]. Poly(ε-caprolactone)/HAP/gelatin nanocomposite was synthesized using an *in situ* co-precipitation method [23]. Moreover, HAP/starch [24], HAP/SEVA [25], HAP/CDHA [26], HAP/sodium alginate [27], HAP/hydrogel [28], HAP/gelatin [29], HAP/collagen [30], CNT/HAP [31], HAP/Ag [32], and collagen/chitosan/HAP nanocomposite [33] γ-Fe_2O_3/HAp-$(CH_2)_3$-$NHSO_3H$ [34] have been developed. Correspondingly, the incorporation of graphene-based materials with HAP nanocomposites, including GO/HAP [35], GO/HAP/CS [36], GO/HAP/SA [37] GO/HAP/poly (vinyl alcohol) [38] have been studied.

In the present study, a novel ternary graphene oxide/hydroxyapatite/silver (GO/HAP/Ag) nanocomposite was prepared, for the first time, by a facile hydrothermal route. The obtained nanocomposite was analyzed by Fourier transform infrared (FT-IR) spectra, Raman spectroscopy, X-ray diffraction (XRD), scanning electron microscopy (SEM), transmission electron microscopy (TEM), ultraviolet visible (UV-Vis) spectroscopy and energy-dispersive X-ray (EDX) spectroscopy. All results showed that this approach is suitable for preparing graphene-based ternary nanocomposite. The catalytic and antibacterial activities of the as-synthesized ternary GO/HAP/Ag nanocomposite were also evaluated. The nanocomposite exhibited high catalytic performance in the reduction of nitro compounds (4-nitrophenol, 2-nitrophenol, 4-nitroaniline, and 2-nitroaniline) using $NaBH_4$ in aqueous medium and at room temperature. To our knowledge, there is no report on the use of rGO/HAP/Ag ternary nanocomposite for the rapid reduction of organic nitrocompounds, especially in the presence of $NaBH_4$ as an environment friendly reducing agent. Additionally, the results showed that this novel ternary nanocomposite has high antibacterial activity against Gram-positive bacteria.

EXPERIMENTAL

Materials

Calcium nitrate tetra hydrate ($Ca(NO_3)_2.4H_2O$, 98%), diammonium hydrogen phosphate ($(NH_4)_2HPO_4$, 98.5%), silver nitrate ($AgNO_3$, 98%), ammonium hydroxide (NH_4OH, 25%), 4-nitrophenol (98%), 2-nitrophenol (99%), 4-nitroaniline (98%), 2-nitroaniline (99%), sodium borohydride ($NaBH_4$, 98.5%), Sodium hydroxide (NaOH), tri-sodium citrate ($C_6H_5Na_3O_7.5.5H_2O$, 98%), ammonium iron (II) sulfate hexahydrate ($(NH_4)_2Fe(SO_4)_2.6H_2O$, 98%) were obtained from Merck chemical company. All of the chemicals were used without further purification.

Synthesis of graphene oxide nanosheets (GO)

Graphene oxide (GO) was prepared by the modified Hummers method through the oxidation of graphite powder [39]. Graphite powder (2.0 g) and $NaNO_3$ (1.0 g) were mixed with 40 mL of concentrated H_2SO_4 in a 500 mL flask and stirred for 1 h in an ice bath. Then $KMnO_4$ (6.0 g) was added into the vigorously stirred suspension slowly below 15°C. The ice bath was then removed, and the mixture was stirred at room temperature until it slowly became brownish slurry. It was diluted with 100 mL of water. The reaction temperature

was rapidly increased to 98°C with effervescence, and the color changed to brown. After that, 200 mL of water and 20 mL of H_2O_2 (30 wt.%) were added. For purification, the mixture was centrifuged and washed with 10% HCl and then deionized water was added several times to remove the residual metal ions and acid. After centrifuging and drying at room temperature, GO was obtained as a powder.

Synthesis of GO/HAP

0.04g of the as-prepared GO powder was dispersed into 20 ml deionized water by ultrasonic treatment for 2 h and 4.5 ml of $Ca(NO_3)_2{\cdot}4H_2O$ (0.1 M) and 2.7 ml of $(NH_4)_2HPO_4$ (0.1 M) were added to the suspension, obtaining Ca/P molar ratio of 1.67. Thereafter, NH_4OH was added slowly in the system, adjusting the pH of the suspension to 10. The mixture was stirred for 2 h at room temperature. The mixture was subsequently transferred to a 50 mL Teflon-lined autoclave and heated at 120˚C for 24 h. Then, it was put away in order to cool to room temperature naturally. The precipitate was washed with deionized water several times and finally, the product was prepared after it was dried at the room temperature for 24 h. For a comparison, pure phase HAP was also synthesized under the same conditions without adding GO powder.

Synthesis of Ag nanoparticles

In a typical experiment, Ag nanoparticles were prepared by using Grape fruit extract as follows: in a 50 mL round-bottom flask equipped with a magnet bar, 10 ml of aqueous solution of Grape fruit extract was mixed with 25 ml of 10 mM aqueous silver nitrate solution. The mixture was then heated at 55°C under constant stirring for an appropriate time (e.g. 25 min) in an oil bath. The formation process and the optical properties of the silver nanoparticles were identified from both the color change and UV-Vis spectra of the solutions**.** In order to remove the Ag nanoparticles product, the solution was centrifuged at 5500 rpm for 20 min. The precipitate was then washed with deionized water for three times to remove any impurities if any. Finally the washed precipitate was dried in an oven maintained at 60°C for 2 h.

Synthesis of GO/HAP/Ag

The 0.04 g GO was dispersed into 20 ml deionized water by ultrasonic treatment for 2 h. Then, 4.5 ml of $Ca(NO_3)_2{\cdot}4H_2O$ (0.1M), 2.7ml of $(NH_4)_2HPO_4$ (0.1 M), and 5 mL of $AgNO_3$ (40 mM) were added to the solution under stirring. The result suspension was adjusted to pH 10 by NH_4OH and then transferred to a 50 mL Teflon-lined autoclave and heated at 120˚C for 24 h. Other processes like washing and drying were similar to those of GO/HAP.

Characterization techniques

The functional groups present in the samples were recorded by a Schimadzu system FT-IR 160 spectrophotometer in transmission mode from 4000 to 400 cm^{-1} using KBr pellets. Raman spectra of the samples were obtained using a Raman microscope (Model: SENTERRA (2009), Germany) with a laser 785 nm. The XRD patterns of the samples were analyzed on an X-ray diffractometer (PANalytical/X'Pert Pro MPD) using Ni-filtered Cu Kα radiation (λ=1.54059 Å). The UV-Visible absorption spectra of samples were obtained using a double beam UV-Visible spectrometer (Cary 100, VARIAN) operated at a resolution of 2 nm with quartz cells with path length of 1 cm in 200-800 nm range. The morphology and elemental analysis of samples were observed by a MIRA3 TESCAN scanning electron microscope (SEM) equipped with a link energy-dispersive X-ray (EDX) analyzer. Transmission electron microscopy (TEM) observations were determined on a Philips CM120 microscope at the accelerating voltage of 200 kV.

Catalytic reduction tests

For the catalytic reduction of 4-nitrophenol (4-NP) to 4-aminophenol (4-AP) in general, freshly prepared aqueous solution of $NaBH_4$ (0.5 mL, 20 mM) was mixed with aqueous solution of 4-NP (2 mL, 0.2 mM) in the quartz cell (1.0 cm path length and 4 mL volume). Then, 5 mg of RGO/HAP/Ag nanocomposite was added to the aqueous solution containing 4-NP and $NaBH_4$. The color of the solution gradually changed from yellow to colorless, indicating the reduction of 4-NP. The progress of reduction was recorded by UV-Vis spectrophotometry in a range of 200-800 nm. For recycling experiment, the rGO/HAP/Ag nanocomposite was collected by centrifugation, washed with deionized water, and then reused. The reduction of 2-nitrophenol, 4-nitroaniline and 2-nitroaniline were also investigated under the same conditions.

Antibacterial activity tests

The bacterial strain of *Bacillus cereus* (PTCC 1556), *Staphylococcus aureus* (PTCC 1112),

Escherichia coli (PTCC 1330) and *Klebsiella pneumonia* (PTCC 1053) were used to evaluate the antibacterial properties of as-synthesized GO, HAP, rGO/HAP, rGO/HAP/Ag nanocomposite and Ag NPs using modified Kirby-Bauer disk diffusion method. The Bacteria were cultured for 18 h at 37˚C in the Nutrient agar medium and then adjusted with sterile saline to a concentration of 2 ×10^6 cfu/mL. Bacterial suspensions in Petri dishes (8 cm) containing sterile Mueller-Hinton agar (MA) were cultured using a sterile cotton swab. The compounds were dissolved in water and the sterile paper discs of 6 mm thickness were saturated with 35 µl of samples and then placed onto agar plates which had previously been inoculated with the tested microorganisms. Amikacin (30 µg/disk) was used as the positive control. After incubation for 24 h at 37 ˚C the antibacterial activity was measured as the zone of inhibition (mm) around the disc.

RESULTS AND DISCUSSION

Characterization of rGO/HAP/Ag nanocomposite

The compositions of the resulting GO, HAP and rGO/HAP/Ag composites were investigated by FTIR spectroscopy. The FTIR spectrum of GO in Fig.1(a) showed absorption bands at 1037, 1224, 1346, 1726, and 1616 cm^{-1}, which are ascribed to alkoxy C–O stretching vibration, epoxy C–O stretching vibration, C–OH stretching vibration, C=O stretching vibration, and C=C benzene ring mode, respectively. Also, the broad peak around 3334 cm^{-1} was due to the stretching vibration of OH [40]. In the spectrum of the prepared HAP (Fig. 1(b)), the asymmetric stretching vibration (υ_3) and bending vibration (υ_4) modes of PO_4^{3-} ion were detected at around (1031, 1099 cm^{-1}) and (568, 605 cm^{-1}), respectively. The symmetrical stretching vibration modes (υ_1 and υ_2) of PO_4^{3-} ion were also found at around 962 and 468 cm^{-1}, respectively. The stretching and librational modes of the OH^- ions were detected at around 3550 and 634 cm^{-1}, respectively [41]. The FTIR spectrum of the rGO/HAP/Ag nanocomposite (Fig.1(c)) showed that the bands for oxygen-containing functional groups of GO were decreased or even some of them vanished entirely. Moreover, a new absorption band appeared at 1564 cm^{-1}, which may be assigned to the C=C stretch vibration of graphene sheets [26]. The absence of the O-H band at 634 cm^{-1}, compared to HAP and the appearance of the C–O stretch band at 1224 cm^{-1}, indicated the

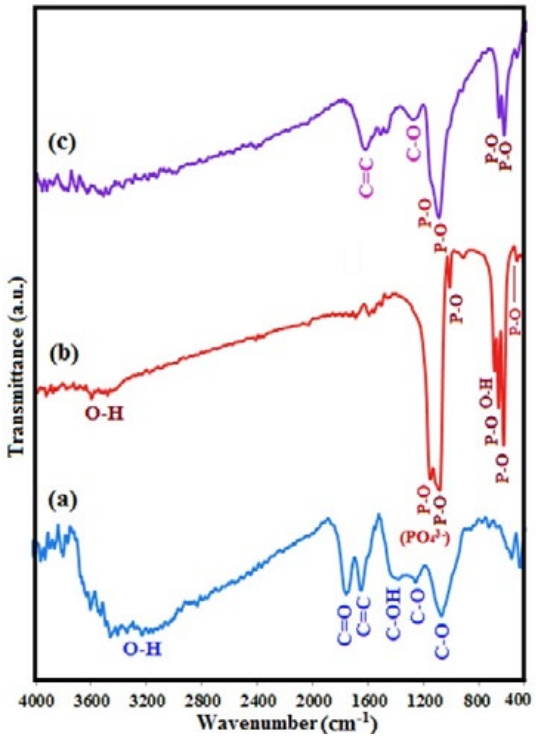

Fig.1. FT-IR spectra of (a) GO, (b) HAP and (c) rGO/HAP/Ag nanocomposite.

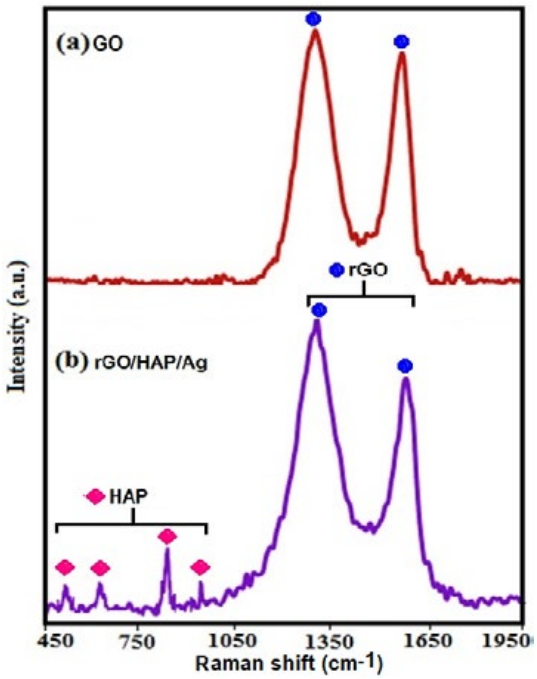

Fig. 2. Raman spectra of (a) GO sheets and (b) rGO/HAP/Ag nanocomposite.

reduction of graphene oxide and formation of the rGO/HAP/Ag nanocomposite.

Raman spectroscopy is a powerful tool to characterize significant structural changes of GO during the composite synthesis. Fig. 2 presents the Raman spectra of GO and rGO/HAP/Ag samples. For pure GO in Fig. 2(a), two characteristic peaks corresponding to the G and D bands of graphene nanosheets were observed at 1590 cm^{-1} and 1318 cm^{-1}, respectively. The G band was assigned to the E_{2g} mode of C sp^2 atoms, while the D band was due to the A_{1g} symmetry and related to the local defects and disorders [40]. As shown in Fig. 2(b), the characteristic two bands of GO in the rGO/HAP/Ag composite appeared at 1594 cm^{-1} and 1319 cm^{-1}, confirming the presence of GO in the nanocomposite. The Raman peaks of the HAP phase were also observed at 470, 572, 960 and 1035 cm^{-1}. These peaks were related to the υ_2 (PO_4^{3-}), υ_4 (PO_4^{3-}), υ_1 (PO_4^{3-}) and υ_3 (PO_4^{3-}) vibration modes of the phosphate groups, respectively [35-36]. The I_D/I_G ratios of GO and rGO/HAP/Ag were found to be 1.09 and 1.25, respectively. It is observed that the I_D/I_G intensity ratio of GO/HAP/Ag are higher than that of pure GO, suggesting a higher level of disorder of the graphene layers during the functionalization process. Raman spectra further confirmed the successful synthesis of rGO/HAP/Ag composite.

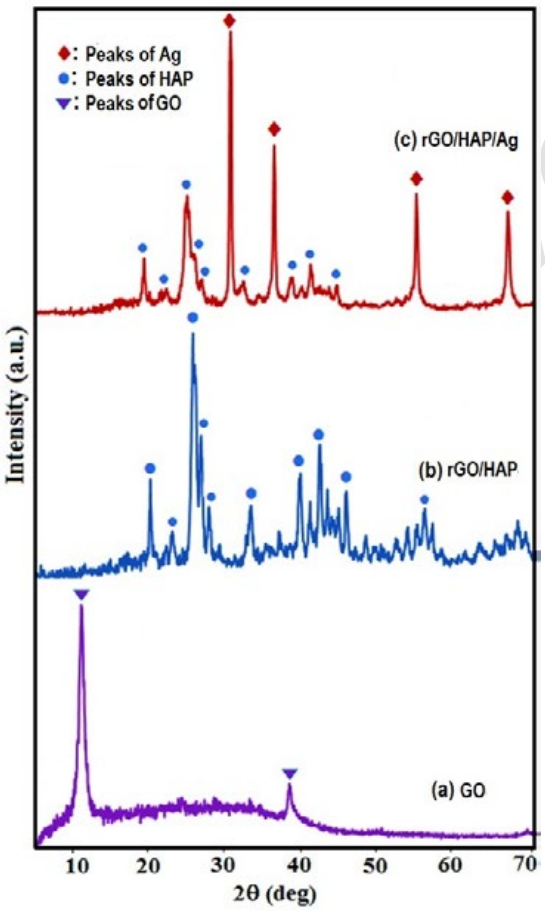

Fig. 3. XRD patterns of (a) GO, (b) rGO/HAP and (c) rGO/HAP/Ag nanocomposite.

Fig. 3 shows the XRD patterns of GO, rGO/HAP, and rGO/HAP/Ag. Fig. 3(a) shows the characteristic speak of GO was observed at 2θ =11˚ which corresponded to the (001) reflection. The diffraction pattern of rGO/HAP in Fig. 3(b) shows characteristic peaks of the HAP hexagonal phase (JCPDS, card number 09-0432). Peaks detected at 2θ around 25.9˚, 32˚, 33˚, 34.1˚, 39.8˚, 46.7˚, and 50˚ were respectively due to the (002), (211), (300), (202), (310), (222), and (321) reflections of HAP [42]. The XRD pattern of rGO/HAP/Ag in Fig 3(c), along with the characteristic peaks of the HAP indicates several diffraction peaks at 38.1˚, 44.3˚, 64.4˚, 77.5˚, corresponding to (111), (200), (220), and (311) reflections of the face-centered cubic (fcc) crystal of the silver nanoparticles (JCPDS, card no. 87-0717) [43]. These results confirmed the formation of hydroxyapatite and silver nanoparticles on rGO. According to the Debye-Sherrer equation, the average crystallite size of rGO/HAP/Ag nanocomposite was calculated to be 25.9 nm. Moreover, no characteristic diffraction peaks of GO were observed in the patterns of binary rGO/HAP and rGO/HAP/Ag nanocomposites, indicating that exfoliated GO nanosheets were not restacked during the synthesis process. Because of the fact that the hydroxyapatite and silver nanoparticles act as the spacers between graphene layers, they cannot be stacked to from a detectable graphitic structure; this consequently weakens the diffraction of single carbon sheets [40].

The UV-Vis spectra for GO, silver nanoparticles, and rGO/HAP/Ag are shown in Fig. 4. As it is indicated in Fig. 4(a), GO show two peaks at 230 nm and 300 nm which is corresponding to the π-π* transition of aromatic C=C bands and n-π* transition of C-O bands, respectively [44]. Pure Ag NPs also showed an absorption peak at 400 nm (Fig. 4(b)). As shown in Fig. 4(c), after a hydrothermal reaction, the peak at 230 nm was red shifted to 260 nm in the rGO/HAP/Ag spectrum, while the peak at 300 nm disappeared. According to this

result, it can be concluded that GO has been reduced to rGO [26]. Moreover, the rGO/HAP/Ag spectrum also showed an absorption peak at 400 nm, indicating that Ag NPs were successfully deposited on the GO sheets.

Fig. 5 shows the SEM images of the as-prepared GO and rGO/HAP/Ag nanocomposite at different magnifications. The SEM micrograph of pure GO in Fig. 5(a) shows the highly porous and layered structure of GO having large stacks, possibly consisting of hundreds of GO nanosheets. It should also be noted that the surfaces of the GO sheets are quite flat and smooth. SEM images of rGO/HAP/Ag in Fig. 5(b-d) show a completely different morphology. It is clearly evident that the nanocomposite product consists of extremely fine particles with sphere-like and rode-like morphologies that appreciably aggregated as clusters due to the extremely small dimensions and high surface energy of the obtained nanoparticles. The SEM images shows GO nanosheets were successfully decorated with the spherical Ag and rod-like hydroxyapatite nanoparticles. Also, these images showed that the hydroxyapatite and silver nanoparticles were homogeneously distributed on the surface of graphene sheets.

The EDX was applied to further characterize the composition of the sample (Fig. 6). The Element analysis (EDX) showed C, O, Ca, P and Ag peaks which, confirmed the presence of GO, HAP and Ag and is consistent with the results obtained from

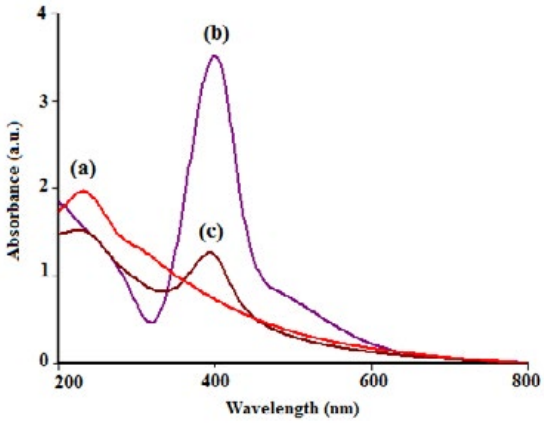

Fig. 4. UV-Vis absorption spectra of (a) GO, (b) Ag nanoparticles and (c) rGO/HAP/Ag nanocomposite.

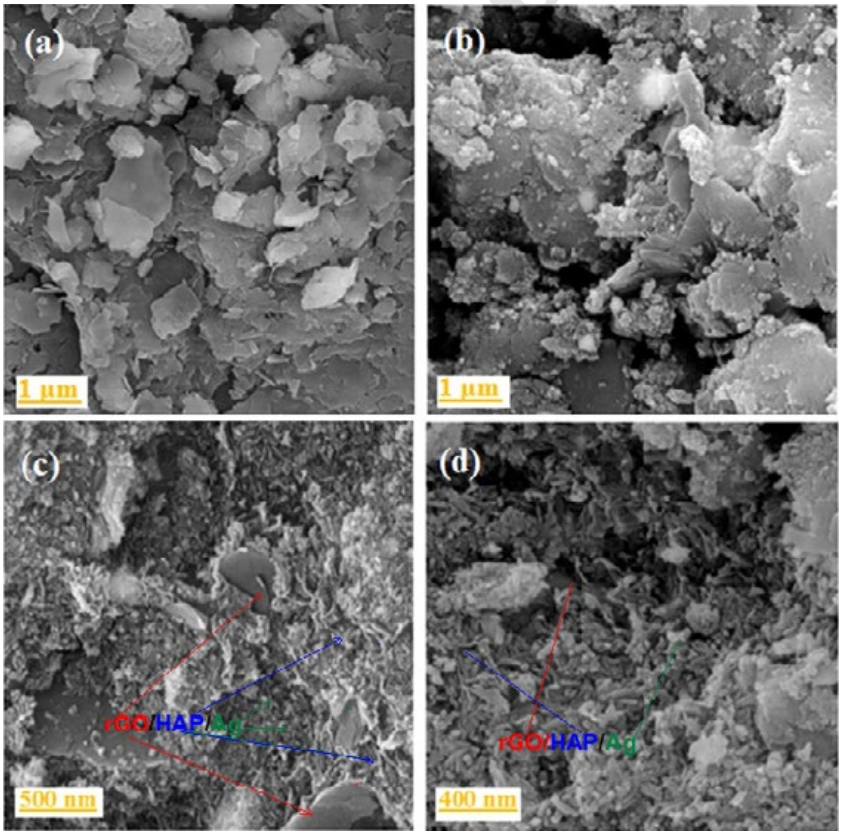

Fig.5. (a) SEM image of pure GO nanosheets and (b)-(d) SEM images of the rGO/HAP/Ag nanocomposite.

XRD patterns. Furthermore the Ca/P atomic ratio of the composite was 1.66, which is very close to the stoichiometric ratio of the pure hydroxyapatite. Moreover, the EDX elemental mapping of the sample in the inset of Fig. 6 displays the uniform distribution of the C, O, Ca, P and Ag elements confirming the homogeneity of the sample.

The TEM images of rGO/HAP/Ag nanocomposite at different magnifications are shown in Fig. 7. The TEM sample was prepared by dispersing the powder in ethanol under the ultrasonic vibration. According to Fig. 7(a-d), large and transparent graphene oxide sheets can be clearly observed in the TEM micrographs. As can be seen in Fig. 7(a-d), the obtained nanocomposite is mainly formed from the rod-like particles and sphere-like particles. In fact, hydroxyapatite nanoparticles contained a rod-like structure while silver nanoparticles showed a sphere-like shape. It can be clearly seen that the hydroxyapatite and silver nanoparticles are well separated and successfully distributed onto the graphene oxide sheets, indicating a strong interaction between graphene and nanoparticles. The average particle size is approximately 26 nm, which is in agreement with the result obtained from the XRD pattern.

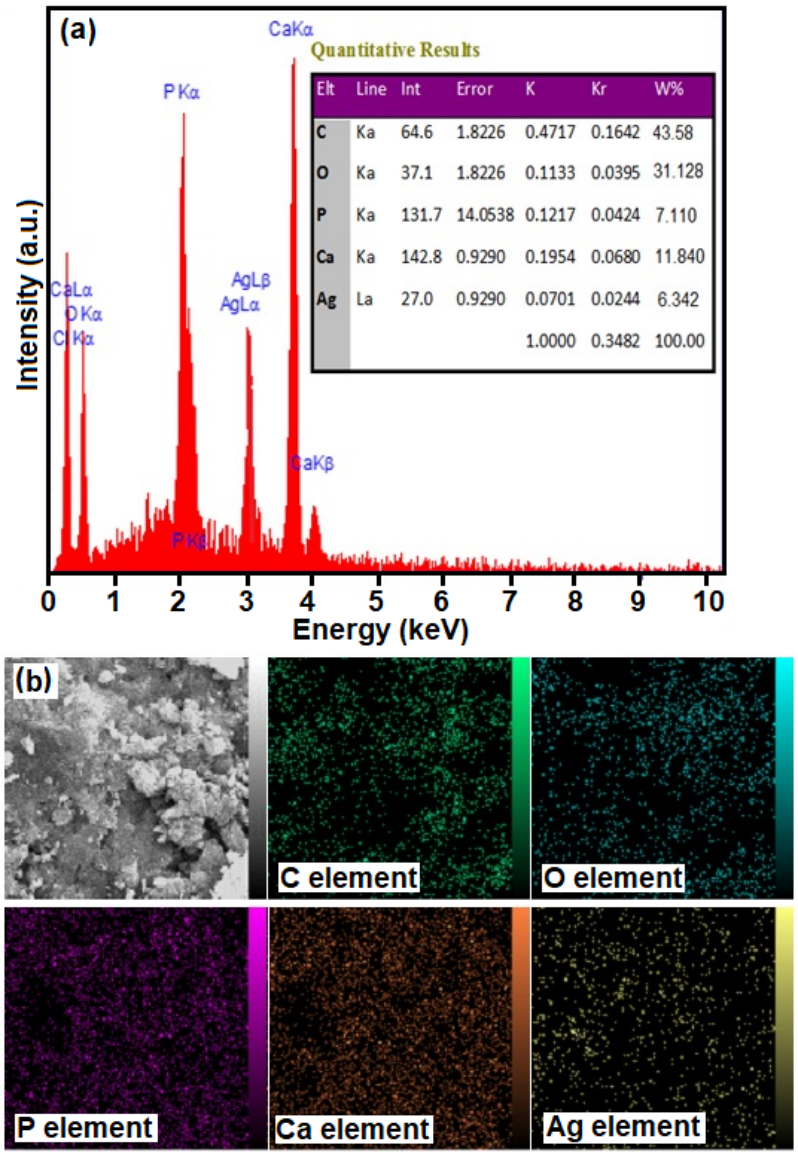

Fig. 6. (a) EDX spectrum of the rGO/HAP/Ag nanocomposite with quantitative elemental analysis (inset) and (b) the elemental mappings of the nanocomposite.

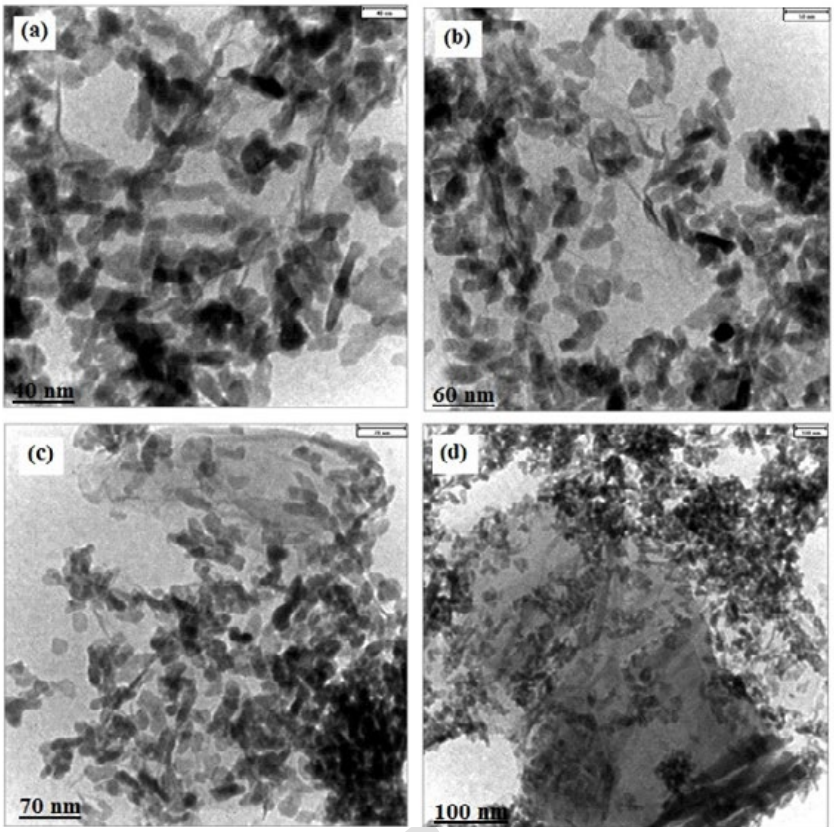

Fig. 7(a)-(d) TEM images of the rGO/HAP/Ag nanocomposite at different magnifications.

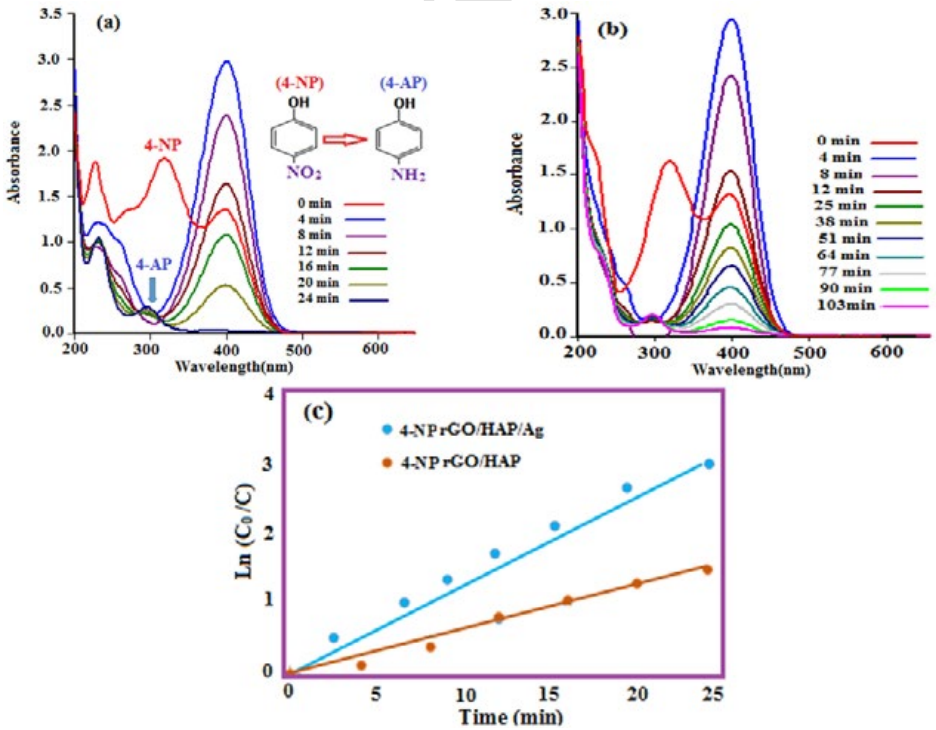

Fig. 8. UV-Vis absorption spectra changes during the reduction of 4-nitrophenol (0.2 mM) with $NaBH_4$ (20 mM) in the presence of (a) rGO/HAP/Ag and (b) rGO/HAP catalyst and (c) plot of $\ln(C_0/C_t)$ against the reaction time.

Catalytic activity of rGO/HAP/Ag nanocomposite

The catalytic reduction of nitrophenols by using $NaBH_4$ as reducing agent in aqueous media has received considerable attention as a relatively simple and clean method [45]. Many reports are available on the application of metal nanocatalysts for the reduction of nitrophenols in the presence of $NaBH_4$. However, the metal nanoparticles are not very stable and easy to aggregate, and thus decrease their activity. In addition, the separation of them from the reaction mixture is an important issue. In order to solve these problems, many researchers are worked on the preparation of nanocomposites which combine the metal nanoparticles with some materials [46-49]. Compared to pure metal nanoparticles, the nanocomposites can be easily separated from the reaction mixture, thus they prevent the loss of catalyst and renders the catalyst cost effective. In such approaches, although nanocomposites showed improved recyclability, they suffered from one or more drawbacks such as the usage of expensive metals (Pt, Pd and Au), and the multi-step preparation procedures. Hence, the development of an alternative inexpensive, facile and easy-removal magnetic catalyst for the reduction of nitrophenols is highly desirable in the context of environmental and industrial concerns.

To evaluate the catalytic ability of rGO/HAP/Ag nanocomposite, the reduction of 4-nitrophenol (4-NP), 2- nitrophenol (2-NP), 4-nitroaniline (4-NA), and 2-nitroaniline (2-NA), with $NaBH_4$ in the presence of rGO/HAP/Ag nanocomposite was examined in aqueous medium and at room temperature. The catalytic reduction process of 4-NP by UV-Vis spectroscopy is shown in Fig. 8(a). 4-NP showed a strong absorption peak at 317 nm. When the $NaBH_4$ solution was added, the absorption peak of 4-NP was shifted from 317 to 400 nm immediately and that was because of the formation of 4-nitrophenolate ions in alkaline condition [50]. The absorption peak at 400 nm remained unaltered for a long duration, suggesting that the reduction did not proceed in the absence of the catalyst. When rGO/HAP/Ag catalyst was added into the solution, the absorption intensity of 4-NP at 400 nm decreased gradually as the time passed by. At the same time, the appearance

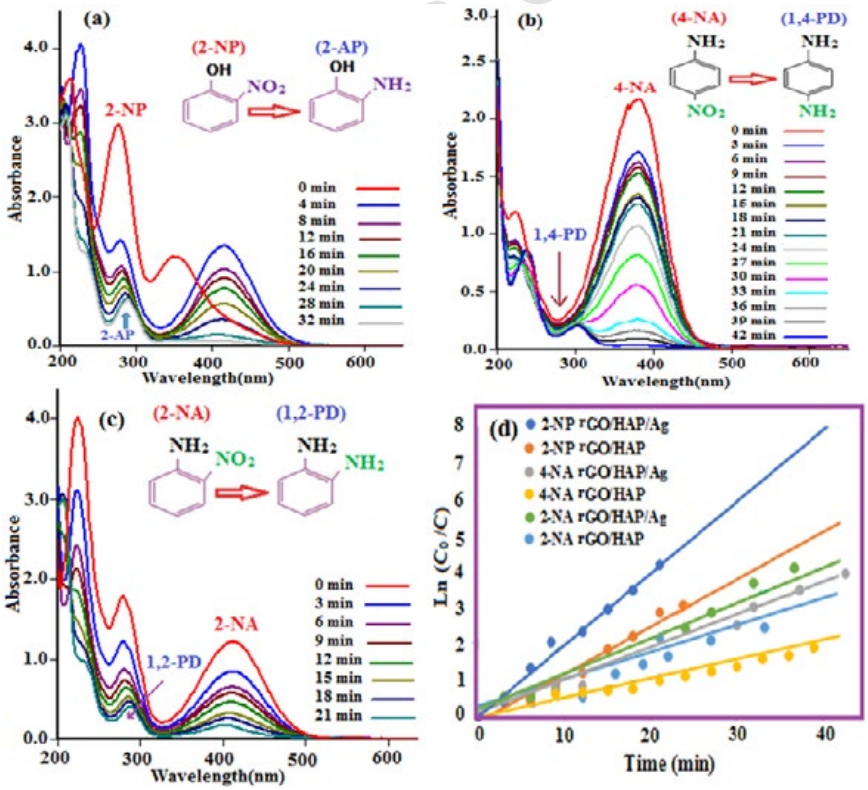

Fig. 9. UV-Vis absorption spectra changes during the reduction of (a) 2-nitrophenol (0.2 mM), (b) 4-nitroaniline (0.2 mM), and (c) 2-nitroaniline (0.2 mM) with $NaBH_4$ (20 mM) in the presence of rGO/HAP/Ag catalyst and (d) plot of ln (C_0/C_t) against the reaction time.

of a new absorption peak at 297 nm indicated the reduction of 4-NP and the formation of 4-aminophenol (4-AP). This reduction reaction, indicated by a fading of the yellow-green color of the reaction solution, completed within 24 min. In addition, rGO/HAP nanocomposite showed low catalytic ability in the reduction of 4-NP as shown in Fig. 8(b). Considering much higher concentration of $NaBH_4$ (20 mM) compared to that of 4-NP (0.2 mM), it is reasonable to assume that the concentration of BH_4^- remains constant during the reaction. In this context, pseudo-first-order kinetics could be used to evaluate the kinetic reaction rate of the current catalytic reaction, together with the UV-Vis absorption data in Fig. 8(c). The absorbance of 4-NP is proportional to its concentration in solution; the absorbance at time t (A_t) and time t = 0 (A_0) are equivalent to the concentration at time t (C_t) and time t = 0 (C_0). The rate constants (k) were determined from the slope of linear plots of ln (C_0 /C) versus time (min). The rate constants (k) were calculated to be 0.1646 and 0.0345min^{-1} for the reduction of 4-NP by rGO/HAP/Ag, rGO/HAP, GO, HAP, and silver nanoparticles (Ag NPs), respectively.

Fig. 9(a) shows the UV-Vis absorption spectra of the reduction of 2-nitrophenol by $NaBH_4$ in the presence of rGO/HAP/Ag nanocomposite. It was seen that the two distinct absorption peaks of 2-nitrophenol at 278 nm and 351 nm shifted to 283 nm and 415 nm, respectively. This change was due to the addition of $NaBH_4$, and consequently the formation of 2-nitrophenolate ions in alkaline condition [51]. When rGO/HAP/Ag catalyst was added into the reaction solution, the absorption intensity of 2-NP at 415 nm decreased gradually with time which proved the reduction of 2-nitrophenolate ions to 2-aminophenol (2-AP). This reduction reaction completed within 32 min. The UV-Vis absorption spectra of the 4-nitroaniline is shown in Fig. 9(b). According to this figure, a strong absorption peak at 380 nm for the 4-nitroaniline can be observed, showing that the intensity gradually decreased as the reaction time increased. Simultaneously, a new peak at 295 nm appeared, which belonged to the characteristic absorption peak of 1, 4-PDA [52]. It took 42 min for the complete reduction of 4-NA in the presence of rGO/HAP/Ag nanocomposite. As it is shown in Fig. 9(c), two peaks of 2-nitroaniline appeared at 283 and 410 nm in UV–Visible range. It was seen that absorption intensity of both peaks was decreased

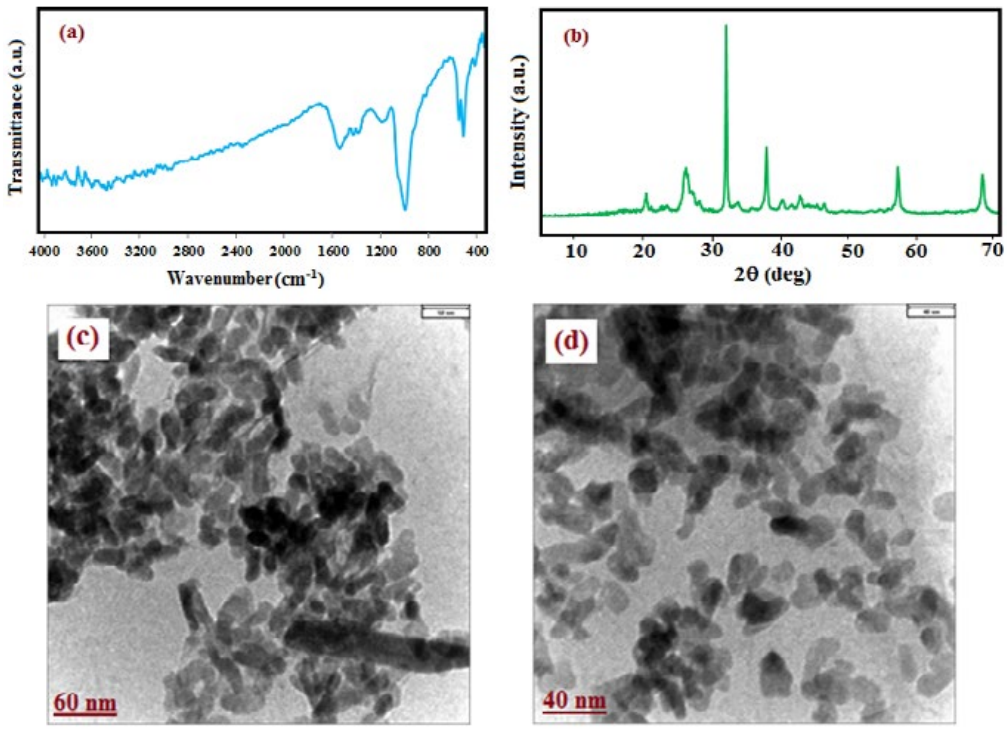

Fig. 10. (a) FT-IR spectrum, (b) XRD pattern, (c) and (d) TEM images of the recovered rGO/HAP/Ag catalyst after four runs of catalytic reaction.

continuously as time passed by, while the peak at 283 nm shifted to 290 nm indicating the formation of 1,2-PDA [53]. After reacting for 21 min, absorption at 410 nm became constant which indicated the completion of the reaction. From Fig. 9(d), the rate constants (k) for the reduction of 2NP, 4-NA and 2-NPwere calculated. The rate constants (k) were determined to be 0.0182, and 0.0898 min^{-1} for the reduction of 2-NP by rGO/HAP and rGO/HAP/Ag, respectively. The value of rate constants (k) were determined to be 0.0096 min^{-1} and 0.1071 min^{-1} for the reduction of 4-NA by rGO/HAP and rGO/HAP/Ag, respectively, and, the values of rate constants (k) were calculated to be 0.0199 min^{-1} and 0.2 min^{-1} for the reduction of 2-NA by rGO/HAP and rGO/HAP/Ag, respectively.

To evaluate the reusability of the rGO/HAP/Ag nanocomposite, the recycling experiments were performed. After the reaction was completed, rGO/HAP/Ag catalyst was separated from the reaction mixture by centrifugation. The catalyst was washed with deionized water and ethanol several times, dried and employed for the next reaction. The activity of the four consecutive runs (98, 97, 95 and 93%) revealed the practical recyclability of the applied catalyst. It was found that 93 % of catalytic activity was retained after reuse for four times, revealing the good stability. After each recycle, the centrifuge supernatant was collected and detected by the Atomic absorption

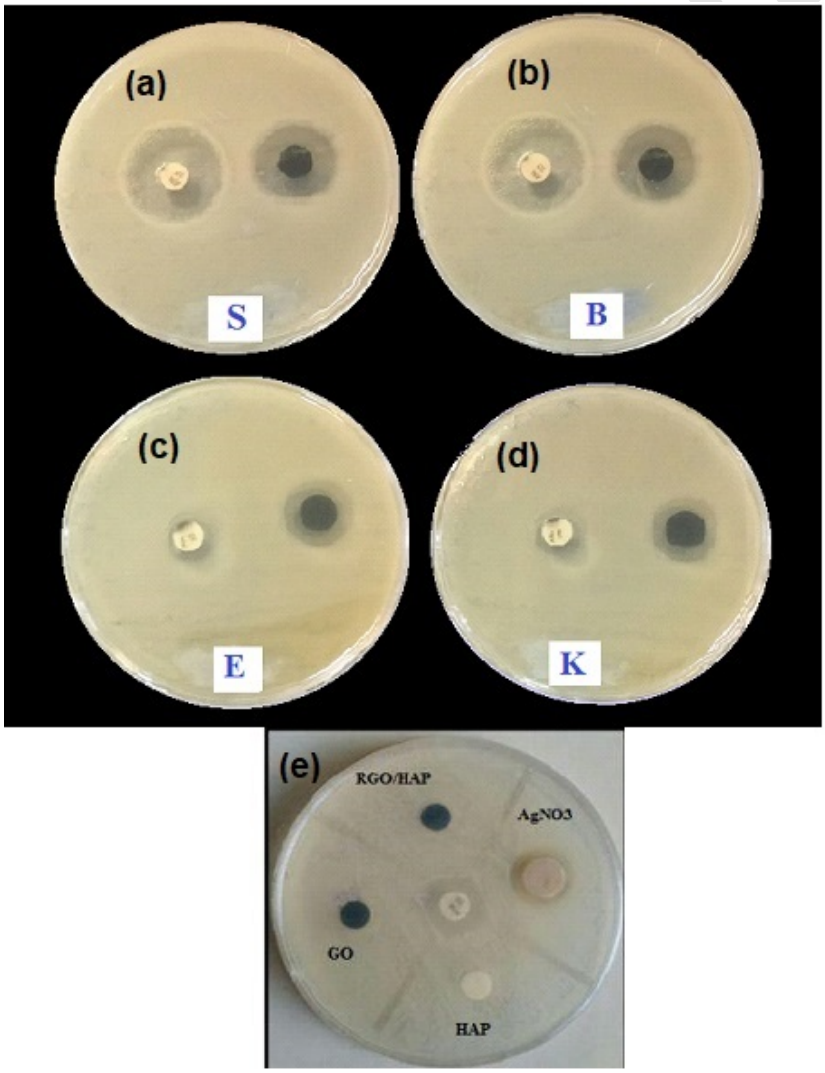

Fig. 11. The images of antibacterial activity of Disc 35 µg/mL rGO/HAP/Ag nanocomposite on (a) *S. Aureus,* (b) *B. Cereus,* (c) *E. Coli*, and (d) *K. Pneumonia.* (e) The antibacterial activity for pure HAP, GO, rGO/HAP and $AgNO_3$ samples.

Table 1. Average of inhibition zone (mm) of rGO/HAP/Ag nanocomposite against different bacterial species.

Entry	Bacteria	Type	Inhibition zone diameter (mm)	
			Nanocomposite	Disk standard
1	*S. Aureus*	Gram-positive	30	17 ± 0.81
2	*B. Cereus*	Gram-positive	28	15 ± 0.52
3	*E. Coli*	Gram-negative	5	12 ± 0.63
4	*K. Pneumonia*	Gram-negative	7	10 ± 0.47

spectroscopy to determine the content of Ag metal. Furthermore, the structural stability the recovered rGO/HAP/Ag catalyst was confirmed by FT-IR, XRD, and TEM after four runs (Fig. 10). As shown in Fig. 10 (a)-(d), FT-IR spectrum, XRD pattern and TEM images of the recycled catalyst did not show significant change after the fourth run in comparison with the fresh catalyst. These observations confirm that the structure of the rGO/HAP/Ag nanocomposite is stable under the reaction conditions and is not affected by the reactants.

Antibacterial activity of rGO/HAP/Ag nanocomposite

Among inorganic antimicrobial agents, silver nanoparticles and its composites have gained more attention due to their broad spectrum antibacterial activities at very low concentrations, suitable safety in usage, good biocompatibility, and intrinsic stability [54]. It is known that although silver substituted HA composites have good antimicrobial response, but, in these composites, a rapid release of silver, depending on the pH, can take place [55]. Because of this fact, Ag nanoparticles have been recently considered as bactericidal reservoir due to their low solubility in aqueous media. Moreover study on polymer films containing Ag nanoparticles reveals that the period of silver release is strongly dependent on the total amount of Ag nanoparticles [56]. The as-synthesized rGO/HAP/Ag nanocomposite was tested for its antibacterial effect against the bacteria strains including *Bacillus cereus*, Staphylococcus aureus, Escherichia coli and Klebsiella pneumonia by disk diffusion method. Fig. 11(a)-(b) shows the results of the antibacterial activity of the rGO/HAP/Ag nanocomposite at the concentration of 35 µg/ml. the average inhibition zones of the bacteria strains are summarized in Table 1. As shown in Table 1, the highest activity of rGO/HAP/Ag nanocomposite was obtained against Gram-positive bacteria *(Staphylococcus aureus* and *Bacillus cereus*) but the inhibition zones of Gram-negative strains (*E. Coli* or *Klebsiella pneumonia*) are very less compared to the standard antibiotic treatment. In control experiments, the antibacterial effects of HAP, GO, rGO/HAP and $AgNO_3$ samples were investigated and as shown in Fig. 11(e) no observable bactericidal activity against bacterial strains was found. According to these results, it can be found that Ag nanoparticles in the ternary rGO/HAP/Ag nanocomposite play a determinant role on the antibacterial effect. The antimicrobial effects of Ag have been known since ancient times. The clear mechanism of Ag nanoparticles interaction with bacteria is not well known. However, several main mechanisms underlie the biocidal properties of Ag nanoparticles against microorganisms. First, Ag nanoparticles in the nanocomposite attach to the negatively charged cell surface, alter the physical and chemical properties of the membrane and wall of cells and disturb important functions such as permeability, osmoregulation, electron transport and respiration [61]. Second, Ag NPs can cause further damage to bacterial cells by permeating the cell, where they interact with DNA, proteins and other phosphorus- and sulfur-containing cell constituents [62]. Third, Ag NPs release silver ions, generating an amplified biocidal effect, which is size- and dose-dependent [63].

It is clear from Table 1 that rGO/HAP/Ag nanocomposite has shown greater antibacterial activity against Gram-positive *bacteria (B. Cereus* and *S. aureus).* The variation in the sensitivity or resistance to both Gram-positive and -negative bacteria populations could be due to the differences in the cell structure, physiology, metabolism, or degree of contact of organisms with nanoparticles [60]. For example, greater sensitivity of Gram-positive bacteria such as *B. Cereus* and *S. aureus* to the rGO/HAP/Ag nanoparticles has been attributed to the greater abundance of thiols, amines and carboxyl groups on their cell surface and greater affinity of Ag towards these groups. Alternatively, Gram-negative bacteria like *E. coli and K. Pneumonia* have a special cell membrane structure which possesses an important ability to resist antimicrobial agents. Furthermore, other factors such as nanoparticle diffusion rates may also affect bacterial strain differently.

CONCLUSIONS

In summary, a novel rGO/HAP/Ag ternary nanocomposite was prepared successfully using a simple and effective hydrothermal method. Graphene oxide sheets were functionalized with hydroxyapatite and silver nanoparticles through a reaction between $Ca(NO_3)_2{\cdot}4H_2O$, $(NH_4)_2HPO_4$ and $AgNO_3$ at 120˚C under hydrothermal conditions. The rGO/HAP/Ag nanocomposite showed better antibacterial activity against the Gram-positive bacteria (Bacillus cereus and Staphylococcus aureus). This nanocomposite was also used as a heterogeneous catalyst for the reduction reaction of 4-NP, 2-NP, 4-NA and 2-NA by $NaBH_4$ in the aqueous solutions. In comparison with rGO/HAP, the rGO/HAP/Ag composite displayed superior activity in this catalytic reaction.

ACKNOWLEDGEMENTS

This work was financially supported by the Lorestan University Research Council and Iran Nanotechnology Initiative Council (INIC).

CONFLICT OF INTEREST

The authors declare that there is no conflict of interests regarding the publication of this manuscript.

REFERENCES

[1] Yang G., (2015), One-pot preparation of reduced graphene oxide/silver nanocomposite and Its Application in the electrochemical determination of 4-nitrophenol. *Int. J. Electrochem*. 10: 9632–9640.

[2] Georgakilas V., Tiwari J. N., Kemp K. C., Perman J. A., Athanasios B. Bourlinos A. B., Kim K. S., and R. Zboril R., (2016), Noncovalent functionalization of graphene and graphene oxide for energy materials, biosensing, catalytic, and biomedical applications*. Chem. Rev.* 116: 5464–5519

[3] Bilton M., Milne S. J., and Brown A. P., (2012), Comparison of hydrothermal and sol-gel synthesis of nano-particulate hydroxyapatite by characterisation at the bulk and particle level. *Open J. Inorg. Non-Metallic Mater.* 2: 1–10.

[4] Sahba R., Sadjadi S. M., Sajjadi A. A., Farhadyar N., Sadeghi B., (2018), Preparation and characterization of friendly colloidal hydroxyapatite based on natural milk's casein. *Int. J. Nano Dimens.* 9: 238-245.

[5] Akhavan K., (2012), Synthesis of hydroxyapatite nanoparticles trough polyelectrolyte-modified microemulsions. *Int. J. Nano Dimens.* 3: 121-125.

[6] Gopi D., Shinyjoy E., and Kavitha L., (2014), Synthesis and spectral characterization of silver/magnesium co-substituted hydroxyapatite for biomedical applications. *Spectrochim. Acta - Part A: Mol. Biomol. Spectrosc.* 127: 286–291.

[7] Ye Q., Ohsaki K., Li K., Li D. J., (2001), Histological reaction to hydroxyapatite in the middle ear of rats. *Auris Nasus Larynx*. 28: 131–136.

[8] Seol Y. J., Kim J. Y., Park E. K., Kim S. Y., Cho D. W., (2009), Fabrication of a hydroxyapatite scaffold for bone tissue regeneration using microstereolithography and molding technology. *Microelectron. Eng.* 86: 1443–1446.

[9] Itokazu M., Yang W., Aoki T., Ohara A., Kato N., (1998), Synthesis of antibiotic-loaded interporous hydroxyapatite blocks by vacuum method and in vitro drug release testing. *Biomaterials*. 19: 817–819.

[10] Sadat-Shojai M., Khorasani M. T., Dinpanah-Khoshdargi E., Jamshidi A., (2013), Synthesis methods for nanosized hydroxyapatite with diverse structures. *Acta Biomater.* 9: 7591–7621.

[11] Blackwood D. J., Seah K. H. W., (2009), Electrochemical cathodic deposition of hydroxyapatite: Improvements in adhesion and crystallinity. *Mater. Sci. Eng. C.* 29: 1233–1238.

[12] Zahouily M., Abrouki Y., Bahlaouan B., Rayadh A., Sebti S., (2003), Hydroxyapatite: New efficient catalyst for the Michael addition. *Catal. Commun.* 4: 521–524.

[13] Bouhaouss M. F. A., Bensaoud A., Laghzizil A., (2001), Effect of chemical treatments on the ionic conductivity of q carbonate apatite. *Int. J. Inorg. Mater.* 3: 437–441.

[14] Mahabole M. P., Aiyer R. C., Ramakrishna C. V., Sreedhar B., Khairnar R. S., (2005), Synthesis, characterization and gas sensing property of hydroxyapatite ceramic. *Bull. Mater. Sci.* 28: 535–545.

[15] Jungbauer A., Hahn R., Deinhofer K., Luo P., (2004), Performance and characterization of a nanophased porous hydroxyapatite for protein chromatography. *Biotechnol. Bioeng*. 87: 364–375.

[16] Lin K., Pan J., Chen Y., Cheng R., Xu X., (2009), Study the adsorption of phenol from aqueous solution on hydroxyapatite nanopowders. *J. Hazard. Mater.* 161: 231–240.

[17] Hashimoto Y., Taki T., Sato T., (2009), Sorption of dissolved lead from shooting range soils using hydroxyapatite amendments synthesized from industrial byproducts as affected by varying pH conditions. *J. Environ. Manage*. 90: 1782–1789.

[18] Poinern G. E., Brundavanam R. K., Mondinos N., Jiang Z. T., (2009), Synthesis and characterisation of nanohydroxyapatite using an ultrasound assisted method. *Ultrason. Sonochem.* 16: 469–474.

[19] Menon D., Anoop Anand K., Anitha V. C., Nair S., (2010), Hydroxyapatite-reinforced polyamide 6, 6 nanocomposites through melt compounding. *Int. J. Polym. Mater. Polym. Biomater*. 59: 498–509.

[20] Pramanik N., Mohapatra S., Bhargava P., Pramanik P., (2009), Chemical synthesis and characterization of hydroxyapatite (HAp)-poly (ethylene co vinyl alcohol) (EVA) nanocomposite using a phosphonic acid coupling agent for orthopedic applications. *Mater. Sci. Eng. C*. 29: 228–236.

[21] Tudorachi N., Chiriac A. P., (2011), Poly(vinyl alcohol-co-lactic acid)/hydroxyapatite composites: Synthesis and characterization. *J. Polym. Environ*. 19: 546–558.

[22] Lowe B., Venkatesan J., Anil S., Shim M. S., Kim S. K., (2016), Preparation and characterization of chitosan-natural nano hydroxyapatite-fucoidan nanocomposites for bone tissue engineering. *Int. J. Biol. Macromol.* 93: 1479–1487.

[23] Hamlekhan A., Moztarzadeh F., Mozafari M.,

Azami M., Nezafati N., (2011), Preparation of laminated poly(caprolactone)-gelatin-hydroxyapatite nanocomposite scaffold bioengineered via compound techniques for bone substitution. *Biomatter*. 1: 91–101.

[24] Sadjadi M. S., Meskinfam M., Jazdarreh H., (2010), Hydroxyapatite - starch nano biocomposites synthesis and characterization. *Int. J. Nano Dimens.* 1: 57-63.

[25] Zhang Z., Fazeli B., (2010), Mechanical properties of SEVA/hydroxyapatite composite with to HAP different particle sizes. *Int. J. Nano Dimens.* 1: 103-109.

[26] Shahmohammadi M., Jahandideh R., Behnamghader A., Rangie M., (2010), Sol-gel synthesis of FHA /CDHA nanoparticles with a nonstochiometric ratio. *Int. J. Nano Dimens.* 1: 41-45.

[27] Rajkumar M., Meenakshisundaram N., Rajendran V., (2011), Development of nanocomposites based on hydroxyapatite/sodium alginate: Synthesis and characterisation. *Mater. Charact.* 62: 469–479.

[28] Zhang L., Rodriguez J., Raez J., Myles A. J., Fenniri H., Webster T. J., (2009), Biologically inspired rosette nanotubes and nanocrystalline hydroxyapatite hydrogel nanocomposites as improved bone substitutes. *Nanotechnol*. 20: 175101(1-12).

[29] Zuo G., Liu C., Luo H., He F., Liang H., Wang J., (2009), Synthesis of intercalated lamellar hydroxyapatite/gelatin nanocomposite for bone substitute application. *J. Appl. Polymer Sci.* 113: 3089-3094.

[30] Kochi A., Kikuchi M., Shirosaki Y., Hayakawa S., Osaka A., (2012), Preparation of injectable hydroxyapatite/collagen nanocomposite artificial bone. *Key Eng. Mater.* 493–494: 689–692.

[31] Bhattarai S. R., Aryal S., Bahadur K. C. R., Bhattarai N., (2008), Carbon nanotube-hydroxyapatite nanocomposite for DNA complexation. *Mater. Sci. Eng. C*. 28: 64–69 .

[32] Akhavan E. A. A., Sheikh N., Khoylou F., Naimian F., (2014), Synthesis of antimicrobial silver/hydroxyapatite nanocomposite by gammairradiation. *Radiat. Phys. Chem.* 98: 46–50.

[33] Wang X., Tan Y., Zhang B., Gu Z., Li X., (2009), Synthesis and evaluation of collagen-chitosan- hydroxyapatite nanocomposites for bone grafting. *J. Biomed. Mater. Res.-Part A*. 89: 1079–1087.

[34] Dadgar M., Milani-Kalkhorani N., (2015), [γ-Fe_2O_3/HAp-$(CH_2)_3$-$NHSO_3H$] nanoparticles as a highly efficient and magnetically separable catalyst for green one-pot synthesis of 4(3H)-Quinazolinones, 6: 473-478.

[35] Lee J. H., Shin Y. C., Jin O. S., kang S. H., (2015), Reduced graphene oxide-coated hydroxyapatite composites stimulate spontaneous osteogenic differentiation of human mesenchymal stem cells. *Nanoscale*. 7: 11642–11651.

[36] Shi Y. Y., Li M., Liu Q., Jia Z. J., Xu X. C., Cheng Y., Zheng Y. F., (2016), Electrophoretic deposition of graphene oxide reinforced chitosan–hydroxyapatite nanocomposite coatings on Ti substrate. *J. Mater. Sci. Mater. Med.* 27: 1–13.

[37] Xiong G., Luo H., Zuo G., Ren K., Wan Y., (2015), Novel porous graphene oxide and hydroxyapatite nanosheets-reinforced sodium alginate hybrid nanocomposites for medical applications. *Mater. Characterization*. 107: 419-425.

[38] Cheng Q., Lan Q., Liu C., Zhao J., (2017), Preparation of graphene oxide reinforced hydroxyapatite Poly (vinyl alcohol) nanocomposite materials. *Interdisciplinary J. Chem.* 2: 1–7.

[39] Kovtyukhova N. J., Ollivier P. J., Martin B. R., Mallouk T. E., Chizhik S. A., Buzaneva E. V., Gorchinskiy A., (1999), Layer-by-layer assembly of ultrathin composite films from micron-sized graphite oxide sheets and polycations. *Chem. Mater.* 11: 771–778.

[40] Rodriguez-Gonzalez C., Cid-Luna H. E., Salas P., Castano V. M., (2014), Hydroxyapatite-functionalized graphene: A new hybrid nanomaterial. *J. Nanomater.* 7: 1-7.

[41] Rajendran A., Barik R. C., Natarajan D., Kiran M. S., (2014), Synthesis, Phase Stability of hydroxyapatite–Silver Composite with antimicrobial activity and cytocompatability. *Ceram. Int.* 40: 10831–10838.

[42] Gu L., He X., Wu Z., (2014), Mesoporous Fe_3O_4/hydroxyapatite composite for targeted drug delivery. *Mater. Res. Bull.* 59: 65–68.

[43] Farhadi S., Ajerloo B., Mohammadi A., (2017), Green biosynthesis of spherical silver nanoparticles by using date palm (phoenix dactylifera) fruit extract and study of their antibacterial and catalytic activities. *Acta Chim. Slov.* 129-143.

[44] Ding G., Xie S., Liu Y., Wang L., Xu F., (2015), Graphene oxide-silver nanocomposite as SERS substrate for dye detection: Effects of silver loading amount and composite dosage. *Appl. Surf. Sci.* 345: 310–318.

[45] Aditya T., Pal A., Pal T., (2015), Nitroarene reduction: A trusted model reaction to test nanoparticle catalysts. *Chem. Commun.* 51: 9410-9431.

[46] Lin F. H., Doong R. A., (2011), Bifunctional Au–Fe_3O_4 heterostructures for magnetically recyclable catalysis of nitrophenol reduction. *J. Phys. Chem. C.* 115: 6591–6598.

[47] Jiang K., Zhang H. X., Yang Y. Y., Mothes R., Lang H., Cai W. B., (2011), Facile synthesis of Ag@Pd satellites–Fe_3O_4 core nanocomposites as efficient and reusable hydrogenation catalysts. *Chem. Commun.* 47: 11924–11926.

[48] He H., Gao C., (2011), Synthesis of Fe_3O_4/Pt nanoparticles decorated carbon nanotubes and their use as magnetically recyclable catalysts. *J. Nanomater.* 2011: 1–10.

[49] Du X., He J., Zhu J, Sun L, An S., (2012), Ag-deposited silica-coated Fe_3O_4 magnetic nanoparticles catalyzed reduction of p-nitrophenol. *Appl. Surf. Sci.* 258: 2717-2723.

[50] Farhadi S., Abroushan E., Zabardasti A., (2017), Ag_3PO_4/$CoFe_2O_4$ magnetic nanocomposite: Synthesis, characterization and applications in catalytic reduction of nitrophenols and sunlightassisted photocatalytic degradation of organic dye pollutants. *RSC Adv*. 7: 18293-18304.

[51] Liu H., Yang Q., (2011), Facile fabrication of nanoporous Au–Pd bimetallic foams with high catalytic activity for 2-nitrophenol reduction and SERS property. *J. Mater. Chem.* 21: 11961-11967.

[52] Guo F., Ni Y., Ma Y., Xiang N., Liu C., (2014), Flower like Bi_2S_3 microspheres: Facile synthesis and application in the catalytic reduction of 4-nitroaniline. *New J. Chem.* 38: 5324-5330.

[53] Farooqi Z. H., Naseem K., Begum R., Ijaz A., (2015), Catalytic reduction of 2-nitroaniline in aqueous medium using silver nanoparticles functionalized polymer microgels. *J. Inorg. Organomet. Polym. Mater.* 25: 1554–1568.

[54] Babu R., Zhang J., Beckman E.J.,Virji M., Pasculle W. A., Wells A., (2006), Antimicrobial activities of silver used as a polymerization catalyst for a wound-healing matrix. *Biomater.* 27: 4304–4314.

[55] Chen K. F., Deng J. H., Zhao F., Cheng G.A., Zheng R.T., (2010), Fabrication and properties of Ag-nanoparticles embedded amorphous carbon nanowire/CNT. *Nanoscale Res. Lett*. 5: 1449–1455.
[56] Lee D., Cohen, R. E., Rubner M. F., (2005), Antibacterial properties of Ag nanoparticle loaded multi layers and formation of magnetically directed antibacterial micro-particles. *Langmuir.* 21: 9651–9659.
[57] Marambio-Jones C., Hoek E. M. V., (2010), A review of the antibacterial effects of silver nanomaterials and potential implications for human health and the environment. *J. Nanopart. Res.* 12: 1531-1551.
[58] Asharani P. V., Mun G. L. K., Hande M. P., Valiyaveettil S., (2009), Cytotoxicity and genotoxicity of silver nanoparticles in human cells. *ACS Nano*. 3: 279-290.
[59] Liu J. Y., Sonshine D. A., Shervani S., Hurt R. H., (2010), Controlled release of biologically active silver from nanosilver surfaces. *ACS Nano*. 4: 6903-6913.
[60] Farhadi S., Ajerloo B., Mohammadi A., (2017), Low-cost and eco-friendly phyto-synthesis of Silver nanoparticles by using grapes fruit extract and study of antibacterial and catalytic effects. *Int. J. Nano Dimens.* 8: 49-60.